

International Journal of Image and Graphics
Vol. 6, No. 2 (2006) 1–26
© World Scientific Publishing Company



AUTOMATIC ACTIVE CONTOURS PROPAGATION IN A SEQUENCE OF MEDICAL IMAGES

KHALIFA DJEMAL

*LSC Laboratory, Université d'Evry Val d'Essonnes
40 Rue du Pelvoux, 91020 EVRY Cedex, France
djemal@iup.univ-evry.fr*

WILLIAM PUECH

*Laboratory LIRMM, UMR CNRS 5506, University of Montpellier II
161, rue Ada, 34392 Montpellier Cedex 05, France
william.puech@lirmm.fr*

BRUNO ROSSETTO

*LOA Laboratory, Université de Toulon et du Var
BP 132, 83957 La Garde Cedex, France
rossetto@univ-tln.fr*

Received

Revised

Accepted

In this paper we present a new algorithm to track an organ in a sequence of medical images in order to achieve a 3D reconstruction. The automatic method that we propose allows the tracking of the external contour of the anatomical organ in all the sequence from one contour initialized by the user on the first image. The required operations for our tracking method are the region-based active contours segmentation. The objects localization with dynamic prediction of displacements is based on the level-set functions and the definition of the region of interest for the robust local estimation of the image model. An application of this method is the 3D reconstruction of abdominal aorta.

Keywords: Sequence of medical images; active contours propagation; automatic segmentation; dynamic prediction of displacement.

1. Introduction

The problem of 3D reconstruction of an object from several images is a classical one that constitutes one of the main problems in computer vision. Many algorithms have been proposed and investigated and a possible solution is to reconstruct 3D object from a set of 2D images.¹ Our work takes place in this case and we are interested in a sequence of images, representing the abdominal aorta, obtained from X-ray computed tomography. An abdominal aortic aneurysm (AAA) is an enlargement of the

2 *K. Djemal, W. Puech & B. Rossetto*

abdominal aorta. Once present, AAAs continue enlarging and become increasingly susceptible to rupture, which usually results in death. Worldwide, approximately 100 000 surgical interventions for AAA repair are performed each year, of which 30% are endovascular. Careful and frequent patient follow-up will likely be needed for the patients after endovascular aneurysm treatment.² The medical 3D reconstruction is important in the detection and follow-up of AAA, among other medical applications, and is the main motivation of this work.

The method we have developed is centered only in the tracking algorithm, which is the first step of a 3D reconstruction. The approach we propose is based on several algorithms and has an objective to track an anatomical organ in a sequence of medical images. The initialization of the tracking algorithm is made only in the first image of the sequence by one initial contour placed by the user. A set of obtained contours is then used for a 3D modeling and reconstruction. Our tracking method is based on active contours segmentation and on automatic localization of objects in a sequence of medical images. This algorithm allows the tracking of an object changing in shape and in topology. The form of the abdominal aorta in a sequence of X-ray computed tomography can be changed by shrinking or dilating. The topology of the object can also change by splitting or merging. Moreover, the image can comprise of other types of organs that may also change in form and even topology. These difficulties motivate us to exclude the idea of taking image of reference in our tracking strategy. In works of Cotes *et al.*³ and Kervrann *et al.*⁴ the way the image is segmented is defined from a parametric form obtained by a training base. Other works⁵⁻⁷ use geodesic active contours requiring *a priori* known form. The propagation is not automatic in all images of the sequence and these methods cannot manage the changes of topology.

One special feature of our method is to track the external contour of the abdominal aorta in a sequence of images. In this aim, we define a region of interest (ROI) for each image of the sequence. We also perform a robust estimation of the image model. On the first image, this ROI is determined by an overall estimation. On the second image, the model is obtained by robust local estimation in the ROI determined by a dilatation of the previous contour. Finally, for other images of the sequence, the ROI is obtained by a dynamic prediction of the displacement from the two previous contours. This dynamic prediction is obtained by the use of the level-set function. The establishment of this method by the level set authorizes changes of topology and an automatic localization of the objects.

In Sec. 2, we expose a review on the active contours methods by presenting the boundary-based and region-based segmentation methods. Firstly, we show that the boundary-based segmentation methods present difficulties on images weakly contrasted and constraints of initialization. Secondly, we recall the region-based segmentation methods which are applied throughout the context of this work. In Sec. 3, we present our automatic propagation method in a sequence of images. Then, we explain the segmentation algorithm and our improvements after we develop the object localization algorithm with robust local estimation. Finally, in Sec. 4, we

apply our method on a sequence of medical images to detect the contours of the abdominal aorta.

2. Active Contours and Our Work Context

Since the work of Kass *et al.*⁸ 15 years ago, two classes of active contours have been developed for the segmentation of objects: Boundary-based and region-based approaches. The first approach uses information located strictly along the boundary. The active contour evolves to the zones with the strongest gradient of intensity. These methods require good initialization. Region-based approaches are powerful tools for the segmentation, where the region-based information must be incorporated in the evolution equation of an active contour. Snakes were introduced by Ref. 8 as an active contour model for boundary segmentation. The model is derived from a variational principle from a non-geometric measure starting from an energy function that includes internal and external terms that are integrated along a curve. Let the curve $C(p) = (x(p), y(p))$, where $p \in [0, 1]$ is an arbitrary parameterization. The snake model is defined by the energy function:

$$E(C) = \alpha \int_0^1 (|C_p|^2) dp + \beta \int_0^1 (|C_{pp}|^2) dp - \gamma \int_0^1 g(C) dp, \quad (1)$$

where $C_p = (\partial_p x(p), \partial_p y(p))$ and α, β, γ are positive constants.

The last term represents an external energy, where $g()$ is a positive edge indicator function that depends on the image $f(x, y)$. This term takes small values along the edges and higher values elsewhere, for example, $g(x, y) = \frac{1}{|\nabla f|^2 + 1}$. The minimum of this energy E is obtained with the curve C , which minimizes E , and the solution of a partial differential equation (PDE).⁸ The snake model is a linear model and thus an efficient and powerful tool for object segmentation and edge integration, especially when there is a rough approximation of the boundary location. However, there is an undesirable property that characterizes this model. It depends on the parameterization. So, the model is not geometric. The geodesic active contour model was introduced by Refs. 9 and 10 as a geometric alternative for the snakes. The model is derived from a geometric function, where the arbitrary parameter p is replaced by an Euclidean arc length $ds = |C_p| dp$.

Indeed, the geometrical and geodesic models allow the independence of the energy function to the parameterization curve which gives more stability to the model of active contour. Then, a convergence towards the nearest solution to the border of the required objects has been obtained. Moreover, the improvements concerning the stop function of active contours are brought. Even if these functions are mainly based on the gradient norm of the original image, they remain relatively powerful if the gradient is very significant. But these methods hardly converge towards an optimal solution, if the image is weakly contrasted. The evolution of the expression can be positive only in determined points, as illustrated in Fig. 1(a), or negative in any points (Fig. 1(b)). Contour can evolve only in one direction during the treatment. The case illustrated in Fig. 1(c), cannot be treated by

4 *K. Djemal, W. Puech & B. Rossetto*

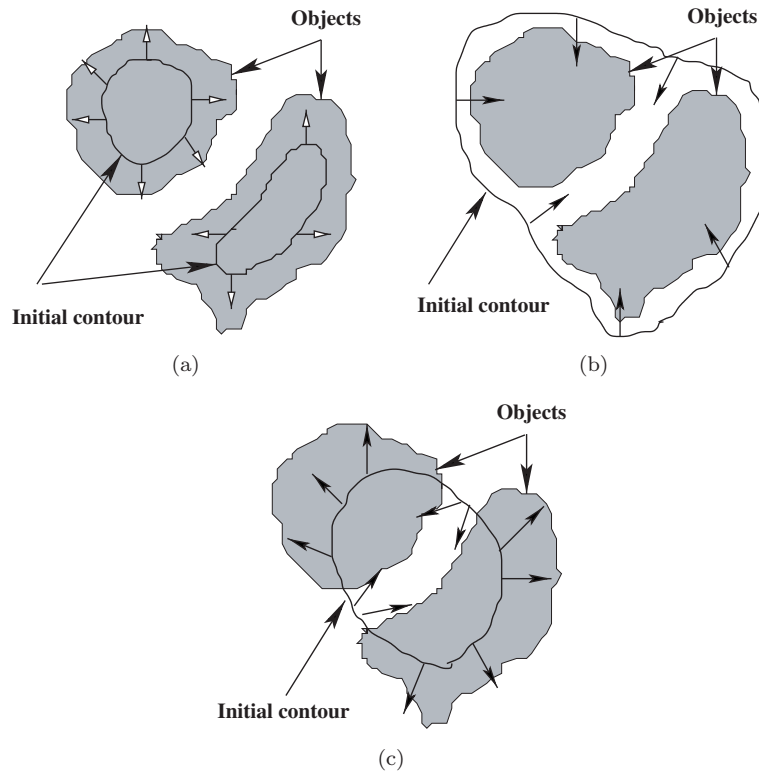


Fig. 1. The different cases of the initialization: (a) Evolution towards the exterior; (b) evolution towards the interior; (c) evolution simultaneous towards the exterior and the interior.

these methods because contours must evolve simultaneously in the two directions. This case can be encountered in an automatic procedure of tracking objects in a sequence of images such as the tracking of the abdominal aorta. The form of this organ can change by shrinking or dilating and the topology can evolve by splitting or merging.

The region-based method consists in defining a criterion where we induce information related to each region in the image. The evolution speed expression is obtained by the minimization of this criterion. Recent studies have shown the potential of these methods for the objects segmentation. Zhu and Yuille^{11,12} have presented a statistical framework for images segmentation. They derived the contour evolution equation by minimizing a generalized Bayes/MDL (Minimum Description Length) criterion inspired from the Mumford and Shah energy.¹³ Paragios and Deriche¹⁴ have proposed an extension of the work of Zhu and Yuille by changing the descriptor function of contour in order to incorporate the image gradient as in geodesic active contour.¹⁰ In their studies, some descriptor functions were evaluated for textures or objects segmentation. Chakraborty *et al.*¹⁵ have introduced a similar region-based approach for the segmentation of medical images. The criterion was

introduced and numerically evaluated to maximize it. In the same way, Chesnaud *et al.*¹⁶ have searched to maximize a likelihood function by choosing at each step the better displacement of the active contour. In these methods the contour is modeled point by point. The management of changes of topology is more delicate and difficult.

Other works have shown that the model of active contour may be improved. Thus the complex forms present in images can be segmented without knowledge precondition of the object topology. Indeed, motivated by the theory of evolution of interfaces (curves), Caselles *et al.*¹⁷ and Malladi *et al.*¹⁸ have introduced geometrical models that take into account internal and external geometrical measurements. From the geometrical model of the active contour, Sethian¹⁹ have introduced the formulation by level set and has shown that this implicit representation makes possible to manage the changes of topology automatically. Treating the case illustrated in Fig. 1(c), one will find difficulties in the calculation of the evolution expression allowing a bidirectional evolution. To solve this problem, Amadiou *et al.*²⁰ have proposed a method which consists in the minimization of a variational criterion of an inverse problem. They have derived the criterion in the distributional sense to obtain the evolution law of the active contour. In our tracking algorithm, the method of segmentation is based on the work of Amadiou *et al.*²⁰ It has the advantage of using only one initial contour. It also allows a formulation by level set to manage the changes of topology.

3. Automatic Propagation in a Sequence of Images

In this section, we present our automatic method of contour propagation in the sequence of images. In Sec. 3.1, we present the region-based active contours segmentation algorithm and our improvements. From the contour resulting of the first image of the sequence, presented in Sec. 3.1, we propose to use it to detect automatically the other contours in all the sequence. In Sec. 3.2, we present the localization algorithm with dynamic prediction of displacements and the determination of the ROI for the robust local estimation of the image model.

3.1. Image modeling and region-based active contours segmentation

As announced in Sec. 2, the method of segmentation is based on the work of Amadiou *et al.*²⁰ starting from the studies of Santosa.²¹ In this section, we recall the principle of this method and we propose some improvements. This method requires the use of partial differential equations (PDE). The utilization of PDE for active contours consists in developing a contour C , according to the following equation

$$\frac{\partial C}{\partial t} = F_c \cdot \vec{N}, \quad (2)$$

where \vec{N} is the normal to C , and F_c a given evolution expression depending on the image model segmentation.

6 *K. Djemal, W. Puech & B. Rossetto*

The active contour C evolves perpendicularly with itself, with an evolution expression F_c until it reaches the edge of the object to be detected. The change of topology can be easily obtained using level-set formulation.^{19,22} In this method, the curve C is defined as the zero level set of a deformable surface u . If C evolves according to Eq. (2), then the surface u evolves following this PDE

$$\frac{\partial u}{\partial t} = F_u \cdot |\nabla u|. \quad (3)$$

A topological change of C does not imply a topological change of u . So, we can detect one or more objects during the same detection process. The model we have chosen to represent the image is

$$f(x, y) = A(I(x, y)) + \eta(x, y), \quad (4)$$

where f is the original image, I the model, A a Gaussian operator and η a noise. The image is defined on a domain Ω with

$$I(x, y) = \begin{cases} I_1/(x, y) \in D_1 = \{(x, y)/u(x, y) < 0\} \\ I_2/(x, y) \in D_2 = \{(x, y)/u(x, y) > 0\} \end{cases}, \quad (5)$$

where

$$D_1 \cup D_2 = \Omega, \quad \text{and} \quad (x, y) \in \Omega. \quad (6)$$

D_1 is the domain of the object and D_2 is the background.

The problem is to find the domain D that corresponds to the model I at convergence, where,

$$\partial D_t = C(t) = \{(x, y)/u(x, y, t) = 0\}. \quad (7)$$

The evolution law of u is defined by the minimization of this criterion:

$$J(t) = \sum_{i=1}^p \int_{\Omega} \|A(I_i(x, y, t)) - f(x, y)\| dx dy, \quad (8)$$

where $\| \cdot \|$ is a norm chosen to optimize the separation of different objects and p the number of domains. In our case we have $p = 2$.

From the original studies²⁰ and our previous experiments,²³ the fastest decrease of $J(t)$ is obtained for evolution expression F_c where,

$$F_c(x, y, t) = \|A(I_1(x, y)) - f(x, y)\| - \|A(I_2(x, y)) - f(x, y)\|, \quad \text{on } C(t). \quad (9)$$

As we can see in Eq. (9), the evolution expression can be positive or negative. Active contours can then evolve simultaneously in both directions, interior and exterior. Thus, the method becomes more flexible and the constraints of initialization decrease, as illustrated in Fig. 1(c).

The PDE (2) becomes:

$$\frac{\partial C}{\partial t} = (\|A(I_1(x, y)) - f(x, y)\| - \|A(I_2(x, y)) - f(x, y)\|)\vec{N}. \quad (10)$$

By taking account of the minimization length of contour,¹⁰ we can consider the new criterion for being minimized in the following way

$$G(t) = \sum_{i=1}^p \int_{\Omega} \|A(I_i(x, y, t)) - f(x, y)\| dx dy + \lambda \int_{C(t)} ds, \quad (11)$$

where λ is a parameter which modifies the influence of the regularization of the contour and ds the Euclidean arc length.

The minimization of $G(t)$ is equivalent to minimize both $J(t)$ given by Eq. (8) and the term of regularization of contour using the same level-set function. The implementation of level set ensures that the topological changes are naturally handled. This allows the detection of all the objects which appear in the image plane without knowing their exact number. The PDE (3) becomes

$$\frac{\partial u}{\partial t} + (F_c(x, y, t) + \lambda \cdot \kappa(x, y, t))|\nabla u| = 0, \quad (12)$$

with κ as the curvature.

As we have shown previously, the evolution expression obtained from Eq. (9) depends on the original image. In order to accelerate the convergence of the algorithm, we define a new evolution expression by affecting it with multiplicative coefficient function of the norm of the gradient of the original image f . The new PDE that allows the evolution of the contour is

$$\frac{\partial u}{\partial t} + (F_c(x, y, t) \cdot |\nabla f|^{\delta} + \lambda \cdot \kappa(x, y, t))|\nabla u| = 0, \quad (13)$$

where $|\nabla f|$ is a numerical evaluation of the norm of the gradient obtained by convolution with the derivative of Gaussian of the image f and a positive constant δ . Its value is given according to the original image. In Fig. 2, the propagation of contour is tested with and without the term $|\Delta f|^{\delta}$ showed in Eq. (13). The convergence with this term is obtained after 273 iterations and without this term the convergence is reached after 315 iterations.

The regularization term λ affects the contour in Fig. 3. For example, with null value for this term (Fig. 3(a)), the propagation is done without regularization. Likewise, for small values of λ , we segment regions which do not correspond exactly to the objects. On the other hand, if we increase this value, the smoothing is more significant, then parts of contours having a strong curvature are disadvantaged (Figs. 3(c) and (d)). Thus we can lose information. The optimal value of λ (Fig. 3(b)), can be chosen by a doctor specialized in medical imaging. The level-set formulation

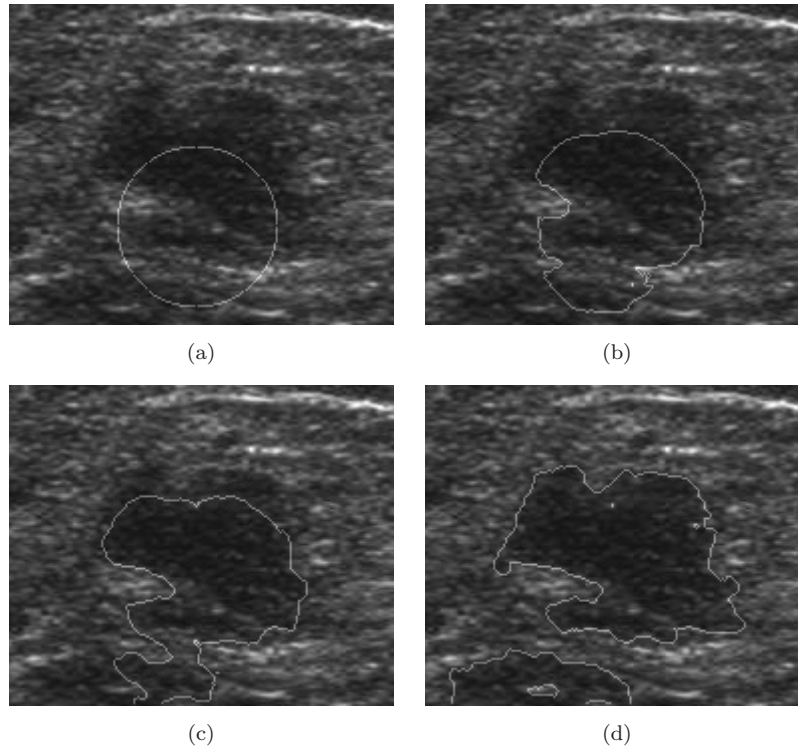
8 *K. Djemal, W. Puech & B. Rossetto*

Fig. 2. Segmentation result on real echographic image representing a breast tumor with optimal regularization term $\lambda = 100$, with the agreement of the radiologist: (a) Initialization; (b) and (c) propagation; (d) convergence, in order to obtain the final contour which represents limit of the breast tumor.

allows an effective estimation of the geometric properties of the contour C as the curvature κ and the unitary normal vector \vec{N} . These properties are estimated by

$$\kappa = \operatorname{div} \left(\frac{\nabla u}{|\nabla u|} \right) \quad \text{and} \quad \vec{N} = -\frac{\nabla u}{|\nabla u|}. \quad (14)$$

In this section, the image $I(x, y)$ is supposed given. This was made possible by a preliminary estimation that was implemented by a robust estimator, presented in Sec. 3.2.2.

3.2. Region of interest and robust local estimation

The principal hypothesis considered in this section is that the variations between two successive cuts of the sequence are weak. In Sec. 3.1, we consider that the image contains two regions, D_1 the objects and D_2 the background. The robust estimation of the image model on the first cut of the sequence is made on the whole image. From the contour obtained from the first image, we define a region of interest (ROI), called ω_2 , for the second image. This ROI contains the desired object and

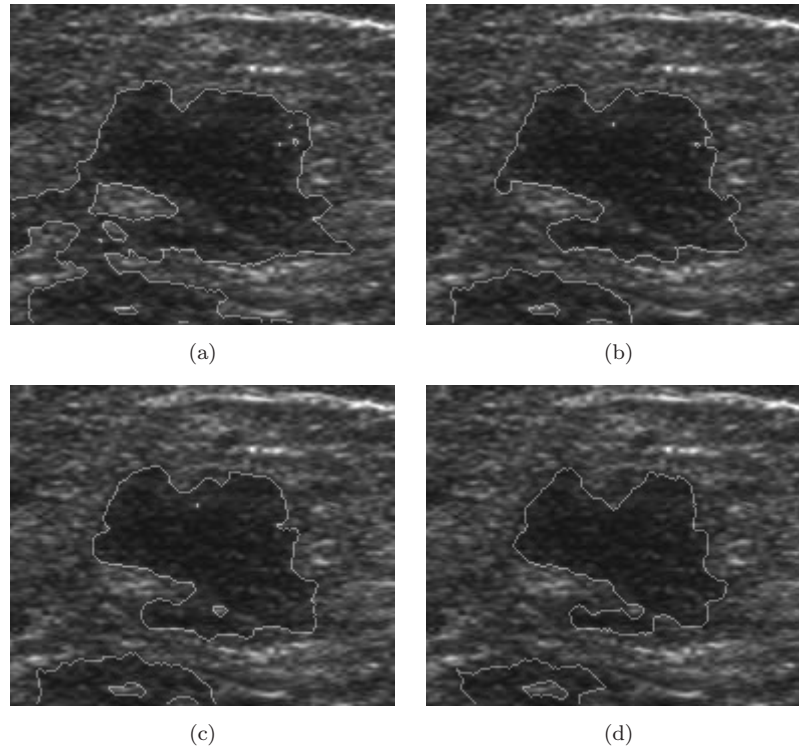


Fig. 3. Effect of the regularization term λ : (a) $\lambda = 0$, convergence without regularization; (b) $\lambda = 100$, convergence with optimal regularization; (c) $\lambda = 200$ and (d) $\lambda = 400$, we much smooth contour and we lose informations.

will allow us to make a robust local estimation of the image model. This ROI for the second image is given by

$$\omega_2 = \beta \cdot \sigma_1^1 = \{(x_0, y_0) + \beta(x - x_0, y - y_0) \mid \forall (x, y) \in \sigma_1^1\}, \quad (15)$$

where β is the dilatation factor with $\beta > 1$ and (x_0, y_0) a point belonging to σ_1^1 . That corresponds to the region of the object in the first image where $\sigma_1^1 = D_1$ as illustrated in Figs. 4(a) and 4(b). In a space of morphological bodies, two basic operators enable us to modify a morphological body. This modification is related to a structured element.²⁴ The dilatation and the erosion are a particular addition and subtraction of the structured element in the morphological body.

The region ω_2 can also be considered by

$$\omega_2 = \sigma_2^1 \cup \sigma_2^2, \quad (16)$$

where σ_2^1 corresponds to the region of the object and σ_2^2 corresponds to the background only in the ROI ω_2 for the second image.

The ROI ω_2 is only a part of the image domain Ω , as illustrated in Fig. 4(c). To get this region, we must firstly fill in the region limited by the contour found in the

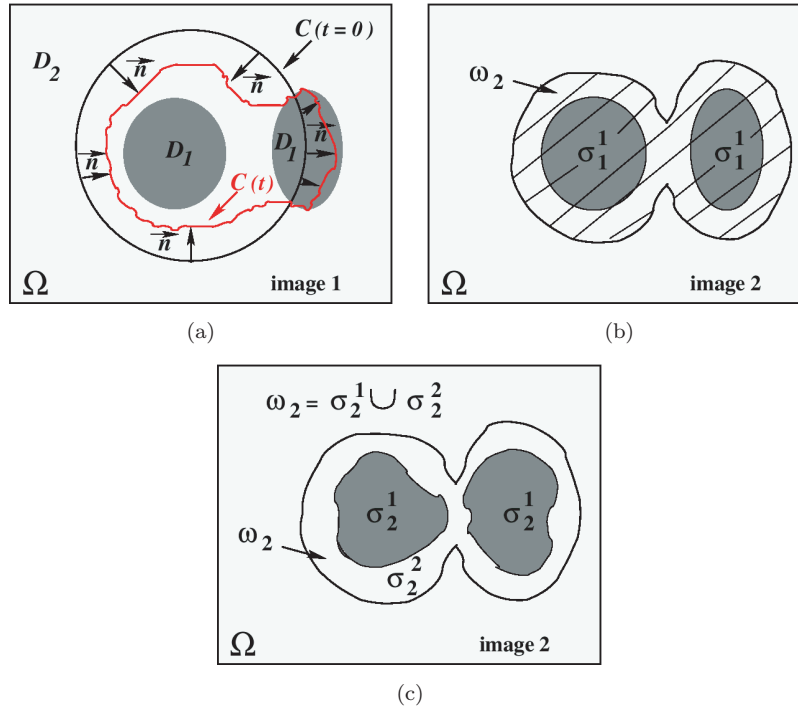
10 *K. Djemal, W. Puech & B. Rossetto*

Fig. 4. (a) Domain of the object and the background in the first image; (b) dilation of the region σ_1^1 of the object of the first image in the second image; (c) propagation of the dilated region from σ_1^1 to get ω_2 , the ROI in the second image.

previous image to obtain σ_1^1 . Secondly, we must dilate this region with a dilatation factor β , as shown in Figs. 4(b) and 4(c).

3.2.1. *Dynamic prediction of displacements and localization*

In this section, we show how a dynamic prediction of displacements to localize the objects is possible. This prediction starts from the third cut. If we consider only the dilation of contours, as we have already shown, several problems encountered. These problems consist in choosing the values of the dilatation factor β adapted to all the images in the sequence. Indeed, if the dilatation is too big, the ROI can contain part of a non-desired object. So, on the other hand, if the dilatation is too small, part of the required object can likely not be in the ROI. To eliminate these problems, we have developed a method of localization by dynamic prediction of displacements of the object on all the sequence. This method is based on the level-set functions. From the third cut of the sequence, we accomplish an estimation of the displacement of the object between the two previous cuts. This estimation makes possible to better define the ROI in which one estimates the image model and to better control the dilatation of contours.

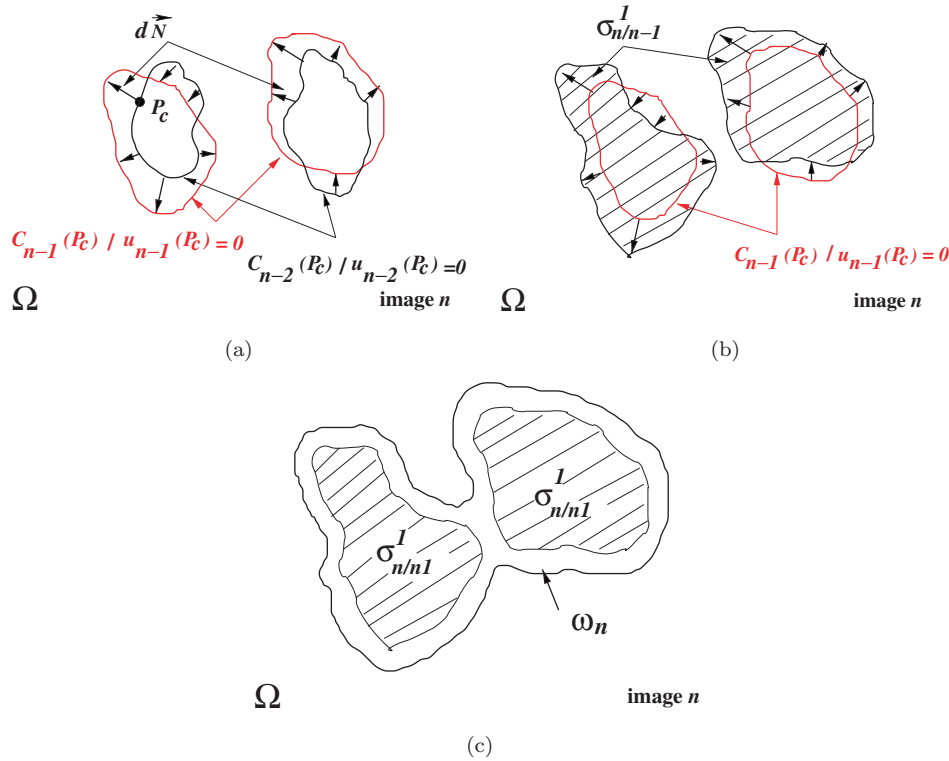


Fig. 5. (a) Displacement estimation between contours C_{n-2} and C_{n-1} such as $(p/u_{n-2}(p) = 0)$ and $(p/u_{n-1}(p) = 0)$; (b) determination of the region $\sigma_{n/n-1}^1$ taking account of the displacement; (c) dilatation of the region $\sigma_{n/n-1}^1$ to get ω_n , the ROI in the image n .

Let p_c be a point of the object boundary in the image $n - 2$. The deformation of object (abdominal aorta) in the image $n - 1$ gives a point belonging to $C_{n-1}(p_c)$. If we note $d(p_c)$, the local displacement of p_c between the images $n - 2$ and $n - 1$, we have $C_{n-1}(p_c) = p_c + d(p_c)$, as illustrated in Fig. 5. Contours $C_{n-1}(p_c)$ and $C_{n-2}(p_c)$ represent respectively the zero level sets of $u_{n-1}(p)$ and $u_{n-2}(p)$. They are the functions obtained at the convergence of the algorithm of segmentation in the two images $n - 2$ and $n - 1$ such that $\{p/u_{n-1}(p) = 0\}$ and $\{p/u_{n-2}(p) = 0\}$. The deformation of the object from the image $n - 2$ to the image $n - 1$ makes the level set function u_{n-2} to evolve towards the level-set function u_{n-1} . We want to estimate the displacement of the object using these functions. We consider the points p_c of the object boundary such as $u_{n-2}(p_c) = 0$. We assume that $p_c + d(p_c)$ belongs to the object boundary in image $n - 1$. So, we have the following equation

$$u_{n-1}(p_c) = u_{n-2}(p_c + d(p_c)). \quad (17)$$

The displacement vector of the point p_c is normal to the direction of the contour $C_{n-2}(p_c)$. Moreover, this displacement is estimated in unitary normal vector sense,

12 *K. Djemal, W. Puech & B. Rossetto*

Eq. (14), as illustrated in Fig. 5(a) with

$$d(p_c) \cdot \vec{N} = [u_{n-1}(p_c) - u_{n-2}(p_c)] \cdot \frac{\nabla u_{n-2}(p_c)}{|\nabla u_{n-2}(p_c)|}. \quad (18)$$

After the displacement estimation, we define an intermediate level-set function, called inter level-set function $u_{n/n-1}(p)$ where

$$u_{n/n-1}(p_c) = u_{n-1}(p_c + d(p_c)). \quad (19)$$

Obtaining the inter level-set function $u_{n/n-1}$ requires an interpolation of the points of the contour obtained from the function u_{n-1} after having taken into account the displacements. This interpolation becomes very difficult if the followed object is divided into several regions, therefore in several contours. To obtain this, and to avoid this interpolation, we define arcs of circles of radius $r = d(p_c)$ of angle α , illustrated in Fig. 6. We consider a circle of center (x_{p_1}, y_{p_1}) and radius r , this can be represented by the following parametrization

$$\begin{cases} x(\theta) = r \cdot \cos \theta + x_{p_1} \\ y(\theta) = r \cdot \sin \theta + y_{p_1}, \quad \theta \in [0, 2\pi]. \end{cases} \quad (20)$$

Then, the arc of circle noted A and centered around the point p_2 (Fig. 6) is denoted by

$$A = \left\{ (x(\theta), y(\theta)) / \theta \in \left[\theta_0 - \frac{\alpha}{2}, \theta_0 + \frac{\alpha}{2} \right] \right\}, \quad (21)$$

where α is given.

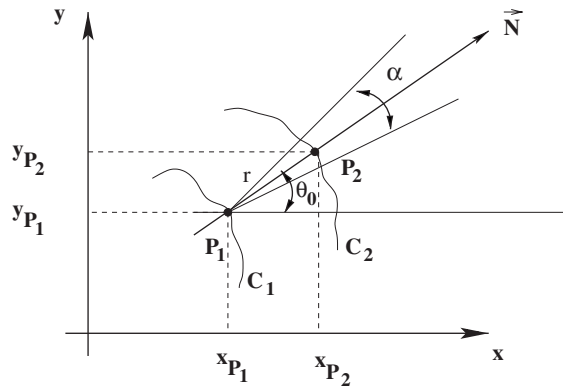


Fig. 6. Definition of the arc of circle, centered around a point of contour.

In this manner, the implementation by level set enables us to manage automatically several contours. The ROI without dilatation, shown in Fig. 5(b), is defined by

$$\sigma_{n/n-1}^1 = ((x, y)/u_{n/n-1}(x, y) \leq 0). \quad (22)$$

Then, the ROI for the image n , illustrated in Fig. 5(c), is obtained by

$$\omega_n = \beta \cdot \sigma_{n/n-1}^1 = \beta \cdot ((x, y)/u_{n/n-1}(x, y) \leq 0). \quad (23)$$

In this region ω_n , we can perform a robust local estimation of the image model. Moreover, that decreases the number of operations and improves the localization of the desired objects.

3.2.2. Robust local estimation

In Sec. 3.1, the image model is represented by the two constants I_1 and I_2 related to the domains D_1 and D_2 , which are respectively the searched object and the background. In this section, we present the advantages of the robust local estimation of the image model. The two constants I_1 and I_2 are estimated on the whole first image with the robust estimator.^{25,26} This estimator is formalized in a weighed least square problem

$$\hat{I} = \text{Arg min} \sum_i \frac{1}{2} \rho_i (f_i - I)^2, \quad (24)$$

with:

$$\begin{cases} \rho_i = \left(1 - \left(\frac{|f_i - I|}{c}\right)^2\right)^2 & |f_i - I| \leq c \\ \rho_i = 0 & |f_i - I| > c \end{cases}, \quad (25)$$

where c represents the maximum value of the residual to limit the contribution of some points and $i \in [1, N]$, if N is the number of pixels in the image.

We have noticed that the variation of the image optical density between two neighboring cuts can change randomly. Furthermore, this global estimation needs more computation time. Beside, it is necessary to remove manually the other objects contained in the global domain Ω of the image, for example, the spinal column.

Moreover, the value of the c parameter should be reconsidered for each image of the sequence. In the case of a robust local estimation with ω_n , the value of c is computed only once from the second image. We can use this value for all images of the sequence. The robust local estimation is only based on the ROI ω_n . In this region, the contribution of the other objects is almost null. This contribution improves the quality of the object estimation and decreases the computing time as illustrated in Table 1, where the time of the estimation can be regarded as inversely

Table 1. Number of pixels in the object and background region for each image of our sub-sequence.

Cuts	Estimation	Total number of pixels ω_n	Background number of pixels σ_n^2	Object number of pixels σ_n^1	Ratio % σ_n^1/ω_n
Cut 1	Entire	65 536	59 006	6530	9.96
Cut 2	Local	21 454	14 536	6918	32.25
Cut 3	Local with	14 775	7465	7010	48.43
Cut 4	prediction	15 761	9176	6585	41.78
Cut 5	(dynamic)	15 158	8612	6546	43.19
Cut 6		15 850	7674	8176	51.59
Cut 7		15 493	8659	6834	44.11

proportional to σ_1/ω_n . From Eq. (24) the robust local estimation of the object is

$$\hat{I}_1 = \frac{1}{\sum_i \rho_i} \sum_i \rho_i I_1. \quad (26)$$

In the case of a robust local estimation, the stability of the c value shows that the background σ_n^2 is a minor part of the local region ω_n . In fact, from the previous cut, we estimate approximately the new region σ_n^1 of the object. Consequently, the robust local estimation is based mainly on the region of the searched object, because the number of points belonging to σ_n^1 is superior to the number of points in σ_n^2 .

4. Experimental Results

In this section, we apply our methods to a part of a sequence of medical images. We use seven cuts (sub-sequence) in the center of this sequence. In Sec. 4.1, we present the result of the active contour propagation on the first image. We illustrate on this sub-sequence the active contour method and the propagation between the first and the second image. In Sec. 4.3, we present results of dynamic propagation on the other images of the sub-sequence.

4.1. Active contour propagation on the first image of the sequence

In Fig. 7, we show the result of segmentation obtained on the first image of sequence of seven cuts representing a part of the abdominal aorta. The evolution is carried out step by step starting from the selected initial shape $u(x, y, t = 0)$ whose zero level set represents initial contour $C(t = 0)$ (Fig. 7(a)). Progressively, with the evolution of the algorithm, the level-set function $u(x, y, t)$ becomes deformed in order to represent contour by taking account of the possible topology changes (Figs. 7(b) and 7(c)). The function evolves until stabilizing itself when the minimum of the criterion (Eq. (11)) is reached. Then, the zero level set represents the final contour of the objects (Fig. 7(d)). The convergence is obtained after 356 iterations with image size of 256×256 pixels. The number of iterations decreases on the other images of the sequence because the initialization is done by the contour obtained

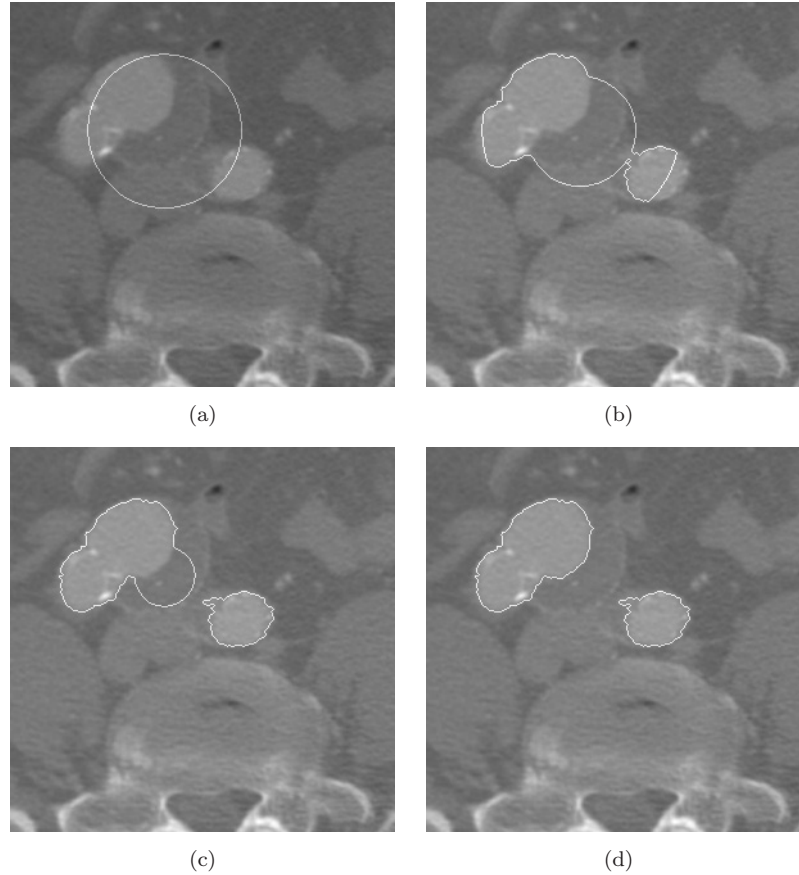


Fig. 7. Segmentation process related to the first cut (image) of the sub-sequence: (a) Initialization by the user; (b) and (c) different steps of the propagation; (d) convergence.

on the previous image. For each application of our segmentation algorithm, the given parameters are the robust estimation of parameter c (described in Sec. 3.2.2) and the regularization term λ . For this first image, the optimal value of regularization term is $\lambda = 150$ with step time $\Delta t = 0.0001$ millisecond. From only one circle that cuts the objects, the evolution expression can be positive in certain points and negative in others. So, the contour can be propagated in the two directions.

The algorithm of segmentation is

Initialization: $\lambda, c, \Delta t, u_{(t=0)}^{i,j}$
Robust_estimation: \Rightarrow image model I_1 and I_2
Compute: evolution expression $F_c^{i,j}$
While convergence is not reached

16 *K. Djemal, W. Puech & B. Rossetto*

Compute: curvature $\kappa_t^{i,j}$ and $|\nabla^{i,j} u_t^{i,j}|$
Compute: $u_{(t+1)}^{i,j}$
Extract contour: $u_{(t+1)}^{i,j} = 0$
Reconstruct: $u_{(t+1)}^{i,j}$

4.2. ROI, robust local estimation and active contour propagation for the second image of the sub-sequence

From the obtained contour of the first image (Fig. 7(d)), we can perform a dilatation of this contour (Fig. 8(a)), to cover completely the surface of the object in the second cut and to obtain the ROI ω_2 (Fig. 8(b)). The robust local estimation of the image model can be done in this ROI ω_2 as illustrated in Fig. 8(c). The used parameter c for the robust local estimation is the threshold which makes it possible to determine the initial value from where an observation is taken as an outlier. Experimentally

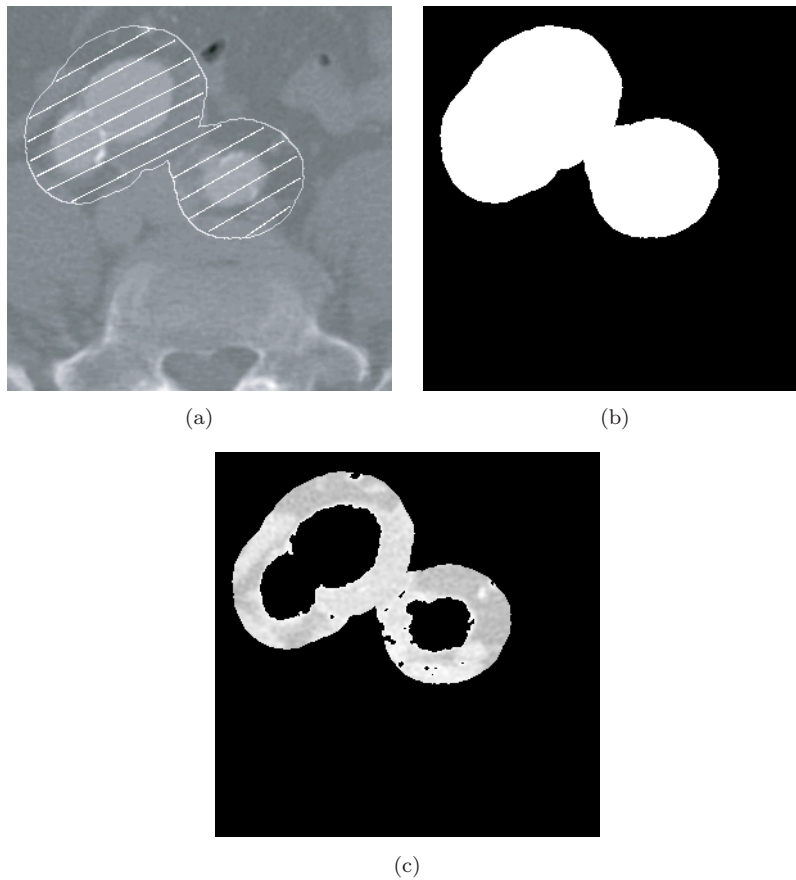


Fig. 8. (a) From the given contour in the first cut (Fig. 7(d)), we have obtained the ROI ω_2 ; (b) filling in the ROI ω_2 to estimate the image model; (c) result of the robust local estimation of the aorta in the second cut.

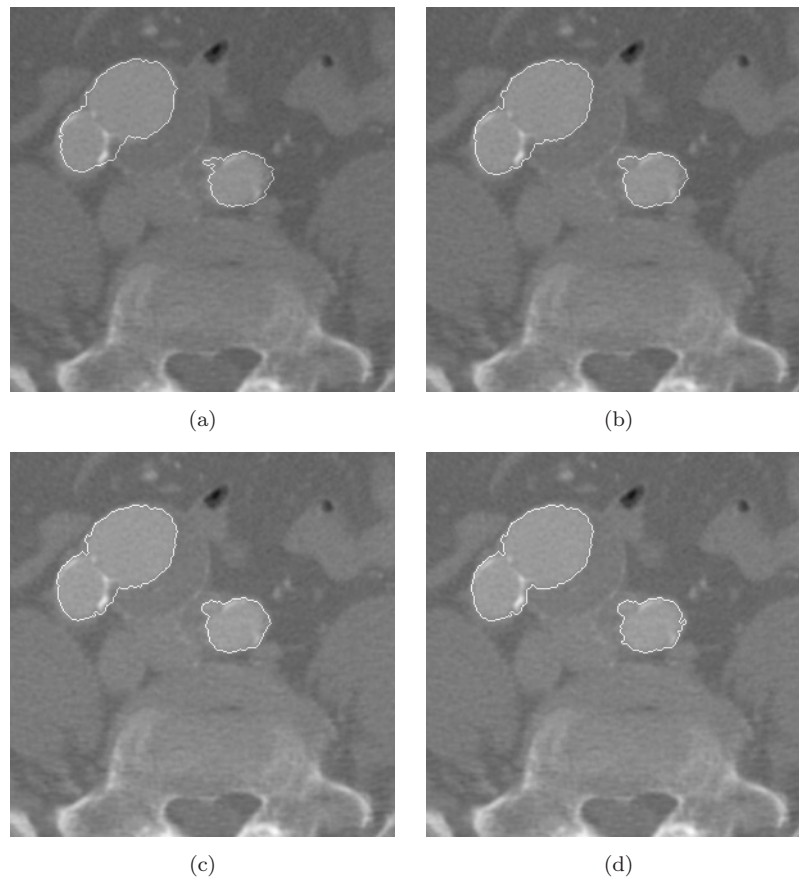


Fig. 9. Segmentation process related to the second image of the sub-sequence, (a) initialization with the contour obtained on the first cut (image), (Fig. 7(d)); (b) and (c) different steps of propagation; (d) convergence in order to obtain the final contour.

in the global estimation, the optimal threshold c belongs to $1 < c < 8$ and this value can change for each image. The interval ($1 < c < 8$) is experimentally limited by estimator of Tokey.²⁵ In the case of an experimentally robust local estimation, we have one optimal value $c = 5$ for all images of the sequence.

We initialize the second image with the obtained contour on the first image (Fig. 9(a)). After propagation (Figs. 9(b) and 9(c)), the algorithm converges on the second image to obtain the contour shown in Fig. 9(d).

4.3. *Dynamic propagation of active contours in the other images of the sub-sequence*

Figures 10(a) and 10(b) illustrate the level-set function u_1 and u_2 respectively for the first and the second images of the sub-sequence. The zero level set of these functions corresponds to the contours of the Figs. 7(d) and 9(d).

18 *K. Djemal, W. Puech & B. Rossetto*

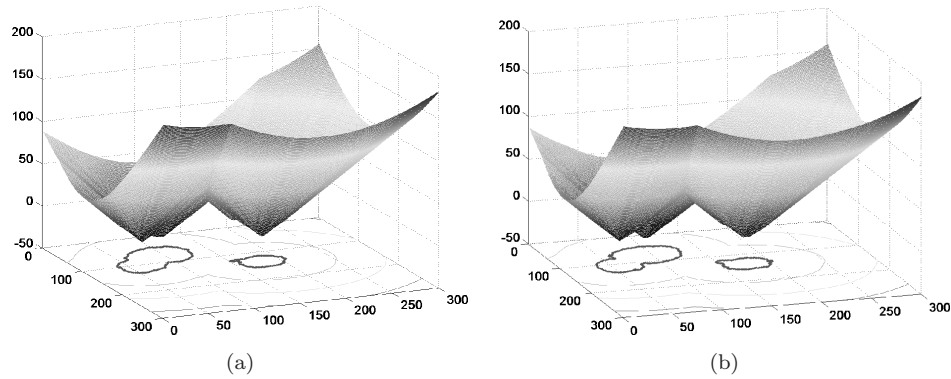


Fig. 10. Level-set functions: (a) The level-set function u_1 after convergence in cut 1; (b) the level-set function u_2 after convergence in cut 2.

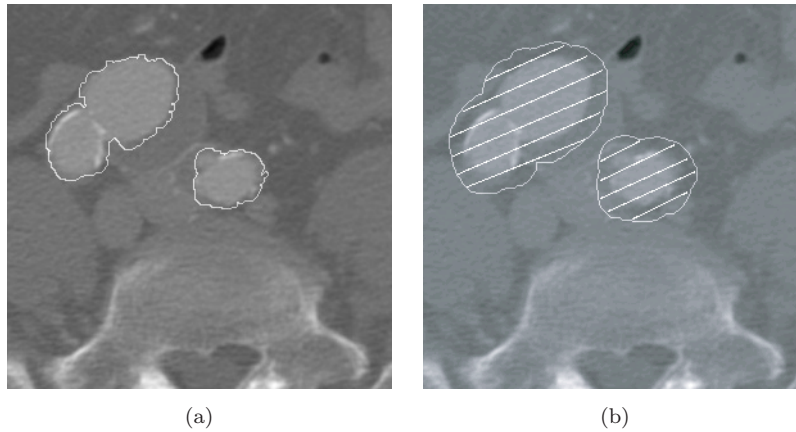


Fig. 11. (a) Result of the dynamic prediction of displacement and localization obtained from the former two cuts to the given $\sigma_{n/n-1}^1$ in the third cut; (b) dilatation with β to obtain the ROI in the third cut; (c) filling in the ROI to estimate the image model; (d) result of the robust local estimation of the aorta in the third cut.

For the third image of our sub-sequence, we estimate the displacement between the first two images to localize the object (Fig. 11(a)). Figure 11(b) illustrates the dilatation to get ω_n .

After filling in the ROI (Fig. 11(c)), we can obtain the robust local estimation of the aorta in the third cut (Fig. 11(d)). So, we do the initialization in the third image with the final contour of the second image (Fig. 12(a)), in order to get the final contour after convergence as it is shown in Fig. 12(b). Figure 13(a) illustrate the ROI obtained after dynamic prediction of displacements and dilatations. Figure 13(c) shows the results of the contours obtained after initialization with previous contours, illustrated in Fig. 13(b), on the fourth, fifth, sixth and seventh cuts of the sequence. In Table 1, we have analyzed for each cut of the sub-sequence the number of pixels in

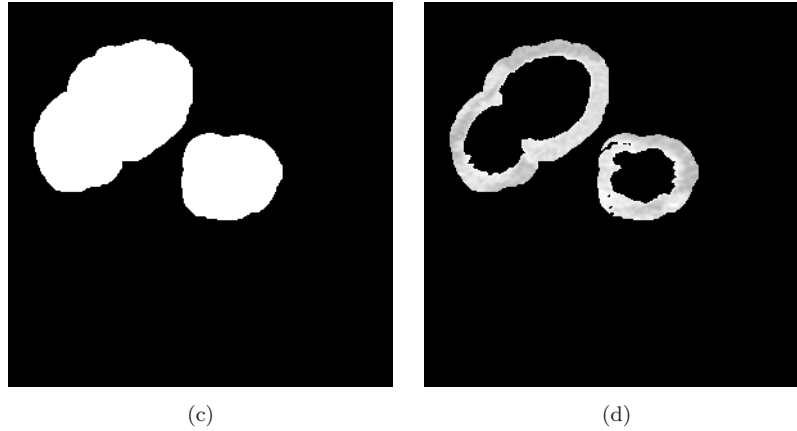


Fig. 11. (Continued)

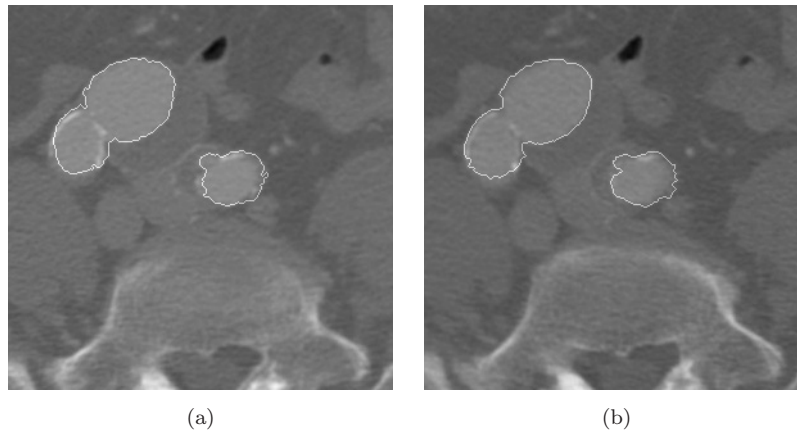


Fig. 12. Segmentation process related to the third cut of the sub-sequence, (a) initialization, on the third cut, with the contour obtained on the second cut (Fig. 9(d)); (b) convergence to obtain the final contour in the third cut.

the object and background regions. We can perceive that the robust local estimation improves the quality of the estimation. Moreover, from the cuts three to seven, with the dynamic prediction, the object region σ_n^1 corresponds about half of the region of estimation ω_n .

The algorithm of localization is:

Obtained level-set functions: from images $n - 2$ and $n - 1$

Compute: displacements between zero level set of u_{n-2} and u_{n-1}

Compute: $u_{n-1} + \text{displacements}$

Construct with interpolation: $\Rightarrow u_{n/n-1} \Rightarrow \sigma_{n/n-1}$

20 *K. Djemal, W. Puech & B. Rossetto*

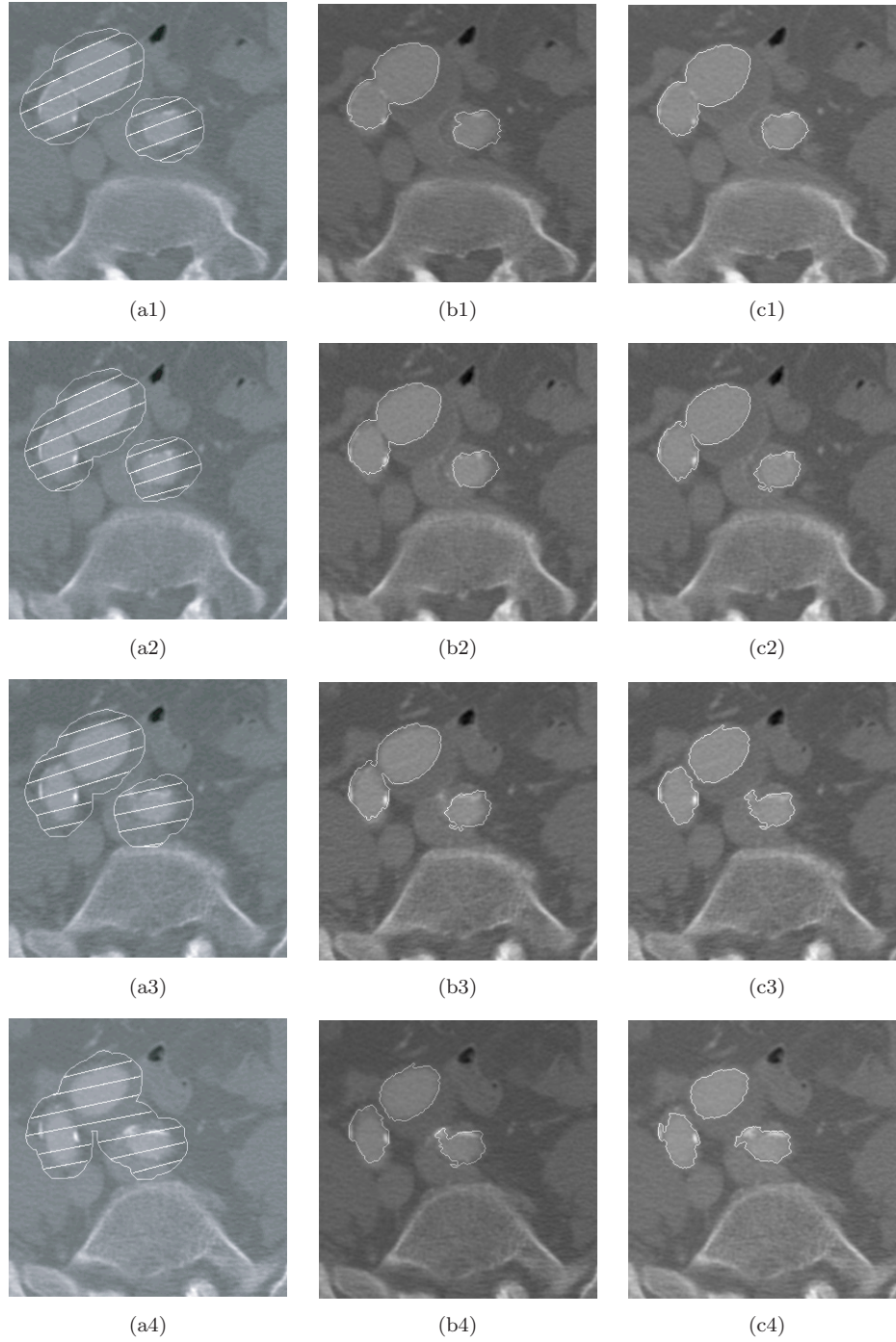


Fig. 13. (a) ROI ω_n ; (b) initialization by previous contours on the fourth, fifth, sixth and seventh cuts of the sub-sequence; (c) convergence and obtained contours.

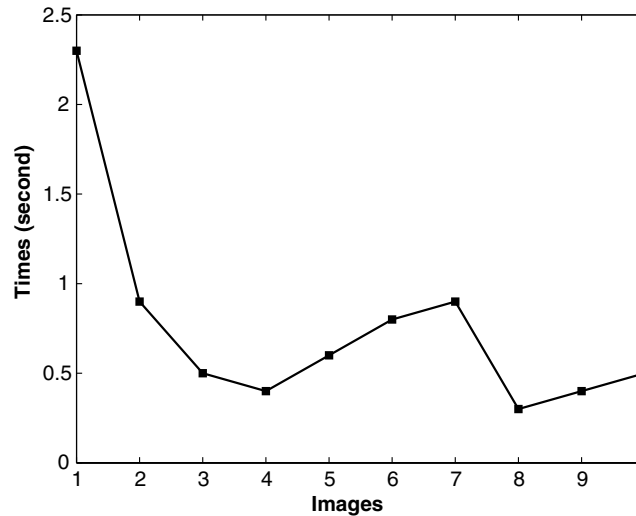


Fig. 14. Time of calculation for ten cuts (images) to get the final contour.

The complete tracking algorithm is:

Segmentation: image ($n = 1$), \Rightarrow zero level set of $u_{n=1} \Rightarrow$ contour 1

Compute: dilatation contour 1 \Rightarrow ROI ω_2

Robust_local_estimation: of image model in ω_2 for image ($n = 2$)

Segmentation: image ($n = 2$), Init. with $u_{n=1}$ (contour 1) $\Rightarrow u_{n=2}$
(contour 2)

While the sequence is not finished $n \leq N$ (N is the number of images)

Localization: $u_{n/n-1}, \sigma_{n/n-1}^1$

ROI: dilatation of $\sigma_{n/n-1}^1$ to obtain ω_n

Robust_local_estimation: image model in ω_n , for image n

Segmentation image n: initialization with u_{n-1} (contour $n - 1$)

We can also observe (Fig. 14), that the necessary time of calculation is more important for the first and second images of the sequence. From the third cut, the time of calculation depends on the displacement between the former two cuts. With the final contours obtained from seven cuts of the sequence, as illustrated in Figures 7(d), 9(d), 12(b) and 13(c) we can perform a 3D reconstruction.

We can see in Fig. 15 three views of this 3D reconstruction. With a sequence of 69 cuts, we can apply our method to get 3D reconstructions of aorta (Fig. 16), obtained from the final contours of the 69 cuts.

5. Conclusion and Discussions

We have proposed a new method of tracking the external contour of anatomical organ from a sequence of medical images. The contour is initialized by the user

22 *K. Djemal, W. Puech & B. Rossetto*

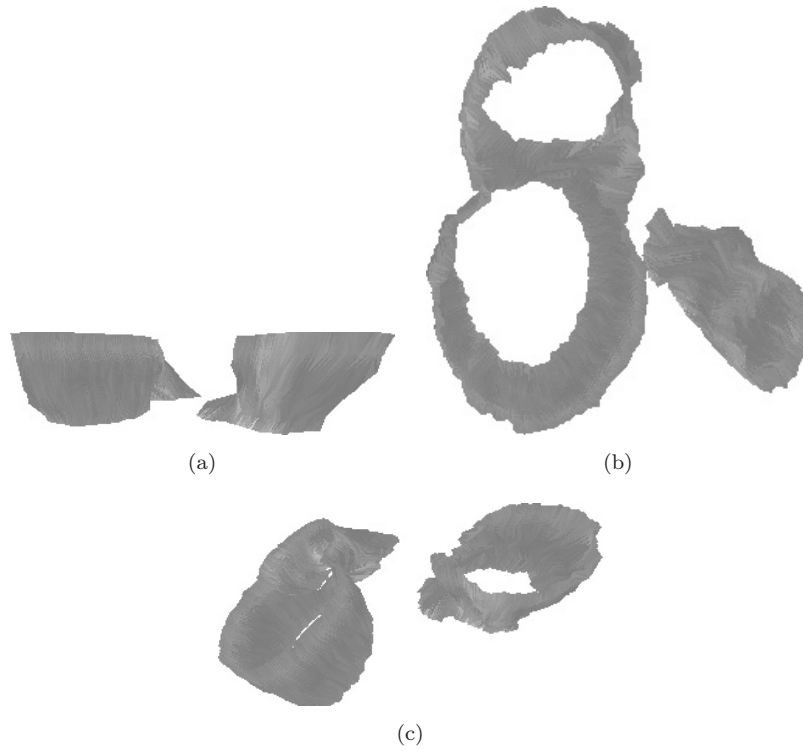


Fig. 15. (a) 3D reconstruction of a part of the aorta obtained from the final contours of seven cuts of the sequence; (b) and (c) two other views of the 3D reconstruction.

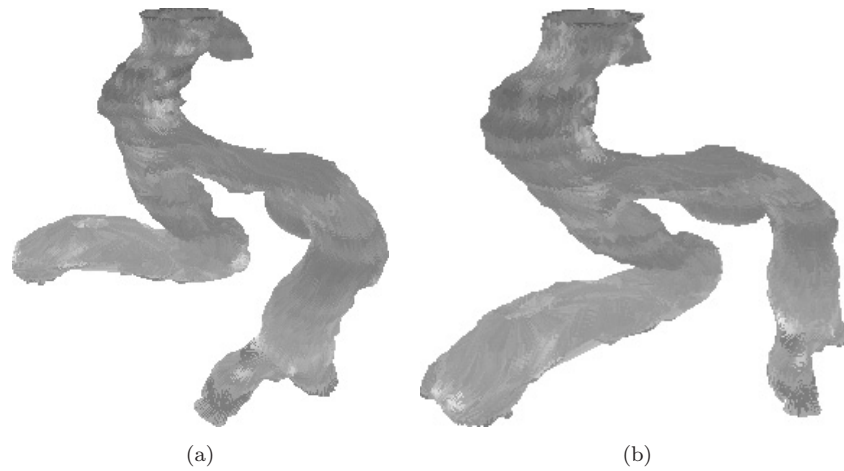


Fig. 16. (a) and (b) Two views of 3D reconstruction of aorta obtained from the final contours of 69 cut sequence.

only on the first image of the sequence. With the results of our method, we can perform a 3D reconstruction of anatomical organ.

A new algorithm for the tracking in a sequence of medical images has been presented in this paper. This method is based on active contours segmentation and automatic object localization. The segmentation algorithm was implemented with level-set methods allows a change of topology and a stable numerical scheme. Moreover, we have shown that the regularization term λ can be chosen by a doctor specialized in medical imaging in order to get a smooth contour.

The dynamic prediction allows us to obtain both a better estimation of the object and to limit the error propagation. Indeed, if the region of interest is obtained by a simple dilatation (β), the preceding contour may have errors that will be taken as part of the object. These errors may cause anomalies of detection of the object on the following images. The dynamic prediction of displacements makes it possible to locate the object, as well as, to determine the ROI.

To estimate the image model, the localization algorithm is based on the dynamic prediction of displacements and the determination of the ROI. The displacements between two consecutive cuts of the sequence are obtained using level-set functions. To perform a robust local estimation of the image model, we have defined an intermediate level-set function. The use of this inter level-set function improves the localization of the desired objects.

To reduce the computation time of the propagation method, it should be possible to parallelize the algorithm of contours detection. In this aim, we can use different methods. It is possible to initialize two contours at both first and last images of the sequence. In this case, the contour propagation is led towards the central cut. Another solution is based on the initialization of the contour on the central image, and the propagation is then done in both directions.

With the obtained contours, we have shown that it is possible to obtain a 3D reconstruction of an anatomic organ. The tracking method we have presented is more automatic than the ones currently used in medical imaging services. This automatic method can be employed for for tele-operations in image processing domain, in order to aid a tediagnosis. Indeed, this reconstruction constitute an important tediagnosis help for the study of the abdominal aorta and of considerable importance for a large number of medical services using 3D imaging techniques. Our method can be applied to other organs in medical applications but also for the temporal follow-up of objects for mobile robots.

Acknowledgments

We would like to thank Professor Agen, responsible of the radiology services at C.H.U. of Toulon for acquiring the X-ray computed tomography images used in our experiments, and for valuable discussions.

24 K. Djemal, W. Puech & B. Rossetto

References

1. R. Berthilsson, K. Astrom and A. Heyden, "Reconstruction of 3D-curves from its 2D-images using affine shape methods for curves," *J. Mathematical Imaging and Vision* (1997).
2. M. Fillinger, "Postoperative imaging after endovascular AAA repair," *Seminars in Vascular Surgery* **12**(4), 327–338 (1999).
3. T. Cotes, A. Hill, C. J. Taylor and J. Haslam, "Use of active models for locating structure in medical images," *Image and Vision Computing* **12**, 355–365 (1994).
4. C. Kervrann and F. Heitz, "A hierarchical statistical framework for the segmentation of deformable objects in image sequence," *IEEE Conf. Comp. Vision Pattern Recognition*, Seattle, USA, pp. 724–728 (1994).
5. M. Fiebich, M. T. Mitchell and K. R. Hoffmann, "Comparison of automatic and manual 3d segmentation in CT angiography of the abdominal aorta," *Scientific Program Radiology Society of North America*, Chicago, Illinois, pp. 474 (1997).
6. M. Jayaraman, B. Kimia, H. Tek, G. A. Tung and J. M. Rogg, "Semiautomated image segmentation of primary brain tumors based on deformable bubbles." *Scientific Program Radiology Society of North America*, Chicago, Illinois, p. 168 (1997).
7. W. Puech, G. Passail and V. Ricordel, "Analysis and optimization of 3D reconstruction method of the aorta from a tomographic images sequence," *Proc. 10th European Signal Processing Conference (EUSIPCO-2000)*, Tampere, Finlande **1** (2000).
8. M. Kass, A. Witkins and D. Terzopoulos, "Snakes: Active contour models," *International Journal of Computer Vision*, pp. 321–331 (1988).
9. V. Caselles, R. Kimmel and G. Sapiro, "Geodesic active contours," *Proc. International Conference of Computer Vision*, Boston, MA, pp. 694–699 (June 1995).
10. V. Caselles, R. Kimmel and G. Sapiro, "Geodesic active contours," *International Journal of Computer Vision*, pp. 61–79 (1997).
11. S. C. Zhu, A. Yuille and T. S. Lee, "Region competition: Unifying snakes, region growing and bayes/MDL for multiband image segmentation," *Proc. Int. Conf. Computer Vision*, pp. 416–423 (1995).
12. S. Zhu and A. Yuille, "Region competition: Unifying snakes, region growing and bayes/MDL for multiband image segmentation," *IEEE Transactions on Pattern Analysis and Machine Intelligence* **18**, 884–900 (1996).
13. D. Mumford and J. Shah, "Optimal approximations by piecewise smooth functions and associated variational problems," *Comm. Pure and Appl. Math.*, **XLII**, pp. 577–685 (1989).
14. N. Paragios and R. Deriche, "Geodesic active regions for motion estimation and tracking," *ICCV*, Corfu, Greece (1996).
15. A. Chakraborty, L. Staib and J. Duncan, "Deformable boundary finding in medical images by integrating gradient and region information," *IEEE Transactions on Medical Imaging* **15**, 859–870 (1996).
16. C. Chesnaud, P. Refregier and V. Boulet, "Statistical region snake-based segmentation adapted to different physical noise models," *IEEE Transactions on Pattern Analysis and Machine Intelligence* **21**, 1145–1156 (November 1999).
17. V. Caselles, F. Catté, T. Coll and F. Dibos, "A geometric model for active contours in image processing," *Numerische Mathematik* **66**, 1–31 (1993).
18. R. Malladi, J. Sethian and B. C. Vemuri, "Shape modeling with front propagation: A level set approach," *IEEE Transactions on Pattern Analysis and Machine Intelligence* **17**, 158–174 (1995).
19. J. A. Sethian, *Level Set Methods*. Cambridge University Press (1996).

20. O. Amadiou, E. Debreuve, M. Barlaud and G. Aubert, "Inward and outward curve evolution using level set methods," *Proc. International Conference on Image Processing, (ICIP-1999)*, Kobe, Japan (1999).
21. F. Santosa, "A Level Set Approach for inverse problems involving obstacles," *ESAIM* (1996).
22. E. Debreuve, M. Barlaud, G. Aubert, I. Laurette and J. Darcourt, "Spice time segmentation using level set active contours applied to myocardial gated," *SPECT Proceeding of Medical Imaging Conference Seattle* (1999).
23. K. Djemal, W. Puech and B. Rossetto, "Active contours propagation in a medical images saquence with a local estimation," *Int. Conf. EUSIPCO-2002*, Toulouse, France (2002).
24. J. Serra, *Image Analysis and Mathematical Morphology*. Academic Press, London **2** (1988).
25. J. M. Odobez and P. Bouthemy, "Robust multiresolution estimation of motion models," *J. Visual Communic. and Image represent.* **6**(4), 348–365 (1995).
26. J. M. Odobez and P. Bouthemy, "Robust multiresolution estimation of motion models in complex image sequences," *Traitement du Signal* **12**(2), (1995).



Khalifa Djemal received the Diploma in optical, image and signal in 1998 from the University of Marseille-Toulon, France and the PhD in image processing in 2002 from the University of Toulon, France.

From 2001 to 2003, he worked as an assistant professor at the Electrical Engineering Department of the Institute of Technology at the University of Toulon. The research field includes development of segmentation algorithms by deformable active contours. The considered applications are mainly related to the tracking of objects in images sequence. Since 2003, he is an associate professor at the Electrical Engineering Department of the Institute of Technology at the University of Evry Val d'Essonne, France. He now works within the T.A.D.I. team of the LSC (Laboratory of Complex Systems). His current research interests is in the areas of image and data processing (Restoration, Segmentation and Clustering).



William Puech received the Diploma of electrical engineering from the University of Montpellier, France, in 1991 and the PhD in signal-image-speech from the Polytechnic National Institute of Grenoble, France in 1997. He initialised its research activities in image processing and computer vision and served as a visiting research associate at the University of Thessaloniki, Greece.

From 1997 to 2000, he had been an assistant professor at the University of Toulon, France, with research interests include methods of active contours applied to medical images sequences. Since 2000, he is an associate professor at the University of Montpellier, France. He now works in

26 *K. Djemal, W. Puech & B. Rossetto*

the Robotic Department of the LIRMM (Laboratory of Informatic, Robotic and Microelectronic of Montpellier). His current interests are in the areas of security of digital image transfer (watermarking, data hiding, compression and cryptography) and edges detection applied to medical images and road security.



Bruno Rossetto received the Master Degree in physics and the PhD Degree in electronics from the Paul Sabatier University of Toulouse, France, and the Doctorat d'Etat in mathematics from the Sud University of Toulon, France, in 1983. Over there he initialised its research activities in periodic differential equations and slow-fast autonomous chaotic dynamical systems. He is a professor since 1995 at the Sud University, and the director of the IUT (Institut Universitaire Technologique) of Toulon since 1997. He now works in a team of the PROTEE Laboratory. His current interests are in the areas of image processing, modelling and chaotic dynamical systems.